Computers and Geotechnics 147 (2022) 104798

Contents lists available at ScienceDirect

Computers and Geotechnics

journal homepage: www.elsevier.com/locate/compgeo

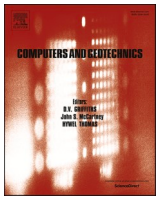

Probabilistic characterization of a high-cycle accumulation model for sands

M. Birrell [a], C. Pastén [b], J.A. Abell [a], R. Astroza [a,*]

[a] Facultad de Ingeniería y Ciencias Aplicadas, Universidad de los Andes, Chile
[b] Departamento de Ingeniería Civil, Universidad de Chile, Chile

ARTICLE INFO

Keywords:
High cycle accumulation model
Ratcheting
Bayesian estimation
Sensitivity analysis

ABSTRACT

In this paper, we employ a Bayesian approach to estimate the parameters of a high cycle accumulation model for sands using experimental data. Global sensitivity analysis and Markov-Chain Monte Carlo simulation are conducted for each of the twenty-four available experimental drained triaxial test results, considering the effect of estimating soil parameters at each strain-cycle under several loading conditions. Probability distributions inferred from each data source are then combined to obtain a single distribution for model parameters. Model calibration is then validated against new observations. The accumulated strain model is calibrated through explicit computation of strain at each cycle and the strain dependence of model parameters is included through the cyclic variation of the model constants.

1. Introduction

Adoption of reliability and risk analyses in geotechnical engineering requires the estimation of input uncertainties (Christian, 2004; Whitman, 1984). In problems solved with numerical simulations where the geomaterial behavior is captured by constitutive models, uncertainties are introduced in the estimation of the model parameters (e.g., Zhou et al., 2021 and examples therein) as well as in the assumptions of the chosen constitutive model. The uncertainty of material parameters can affect the prediction of the performance of embankments (Otake et al., 2021), shallow foundations (Suchomel and Mašín, 2011), tunnels (Miro et al., 2015), excavations (Jin et al., 2020), and slopes (Aladejare & Wang, 2018). For instance, the assessment of uncertainty in model parameters has been studied in the literature for soft soils (Zhou et al., 2018), sands and silts (Jin et al., 2019), and liquefiable sands (Mercado et al., 2019). As a result, the parameters and their probability density functions are estimated to obtain probabilistic model characterizations that consider these sources of uncertainty and how they propagate to model predictions, with the goal of achieving a more realistic numerical representation of actual phenomena.

High cycle accumulation (HCA) models have been developed to predict the long-term response of boundary value problems that involve several low magnitude load or strain cycles (more than $\sim 10^5$ cycles) at a cost-effective computational time. Compared to constitutive models that estimate the residual deformation during cyclic loading by implicitly defining the stress-strain material behavior (Corti et al., 2016; Liu et al., 2019), HCA models explicitly calculate the accumulated shear and volumetric strains as a function of the number of load cycles, the state of stress, and state parameters, such as the current void ratio, among others (Suiker and Borst, 2003; Niemunis et al., 2005; Pasten et al., 2013; Francoise et al., 2006). Some of these models require the verification and update of model parameters at certain load cycles, termed control cycles, using additional constitutive models (Staubach et al., 2021). The use of these constitutive models in geotechnical applications allow the estimation of compatible displacement and stress fields (Staubach et al., 2021; Chong & Pasten, 2018; Machaček et al., 2018). One example of such geotechnical applications is the modelling and prediction of the accumulation of deformation (especially tilt) in offshore wind turbines founded on monopiles (Houlsby, 2016). HCA models have been formulated and successfully applied recently towards this problem (Staubach et al., 2021; Cuéllar et al., 2014; Jostad et al., 2020; Liu et al., 2021), lending credibility to the use of direct nonlinear numerical simulation for high-cyclic response of geotechnical systems. Nevertheless, because these applications target high number of cycles, the response measures of interest are very sensitive to accumulation of errors which, among other obvious sources such as numerical integration issues, may come from uncertainty in the constitutive input parameters themselves calibrated from laboratory tests. Therefore, the study of the uncertainty propagation from lab tests into inferred constitutive parameters used in these problems is of great relevance to understand the uncertainty in the system response, which requires a probabilistic characterization of the input constitutive parameters.

* Corresponding author.
E-mail address: rastroza@miuandes.cl (R. Astroza).

https://doi.org/10.1016/j.compgeo.2022.104798
Received 22 December 2021; Received in revised form 18 March 2022; Accepted 26 April 2022

In this manuscript, we adopt a Bayesian inference-based methodology to calibrate the HCA model proposed by (Niemunis et al., 2005) using available drained cyclic triaxial test results (Wichtmann, 2005). A similar calibration approach was developed for hysteretic reinforcing steel one-dimensional constitutive stress–strain relationships using experimental cyclic tests conducted on reinforcing steel coupons (Birrell et al., 2021). First, the prior distributions are estimated with global sensitivity analysis (GSA) in the form of Sobol's indices. Then, the posterior parameter distributions for *N*-independent and *N*-dependent cases are estimated with Markov Chain Monte Carlo (MCMC). Analyses are performed to evaluate the use of *N*-independent and *N*-dependent approaches. The probabilistic calibration framework for the HCA model presented herein uses all the tests results simultaneously, contrary to sequentially as presented by the model authors (Wichtmann et al., 2010), to estimate the model parameters.

2. Experimental data

The experimental data used for model calibration in this work come from twenty-four cyclic triaxial tests on a coarse sand, generated by Wichtmann (Wichtmann, 2005) and later published by Wichtmann et. al (Wichtmann et al., 2009) and also studied by Pastén et. al. (Pasten et al., 2013). The data consist of accumulated strain measured at 15 different number of stress cycles, control cycles $N = 2, 5, 10, 20, 50, 100, 200, 500, 1000, 2000, 5000, 10000, 20000, 50000$ and 100000. The tested material corresponds to a coarse sand with mean grain size d_{50} of 0.55, uniformity coefficient C_u of 1.8, curvature coefficient C_c of 1.2, loosest (e_{max}) and densest (e_{min}) void ratios of 0.874 and 0.577, respectively, and a critical friction angle φ_c of 31.2.

Four series of six tests each were originally designed by Wichtmann (Wichtmann, 2005) to calibrate the constants of the HCA model. The first series considered variations in the shear stress amplitude q_{ampl}, while other test conditions were kept constant. The second series considered different initial densities, reflected by different initial void ratios e_0. The third series considered variations in stress obliquity η, defined as the ratio of the shear stress $q=(\sigma_v - \sigma_h)$ and the mean effective stress $p=(\sigma_v + 2\sigma_h)/3$. Lastly, the fourth series included different mean pressure values p_{av}, which implied different stress amplitudes to maintain the ratio $\xi = q_{ampl}/p_{av}$ constant at 0.3 and $\eta_{av} = 0.75$.

Table 1
Summary of experimental data.

Series	Test ID	η	p_{av} (kPa)	e_0	q_{ampl} (kPa)	ε_{ampl} (10^{-4})
	1	0.75	200	0.693	22	1.019
	2	0.75	200	0.697	42	2.002
q_{ampl}	3	0.75	200	0.696	51	2.434
	4	0.75	200	0.686	60	2.890
	5	0.75	200	0.685	70	3.381
	6	0.75	200	0.685	80	3.969
	7	0.75	200	0.594	60	2.245
	8	0.75	200	0.619	60	2.424
e_0	9	0.75	200	0.674	60	3.058
	10	0.75	200	0.715	60	2.893
	11	0.75	200	0.729	60	3.526
	12	0.75	200	0.803	60	2.956
	13	0.25	200	0.705	60	2.956
	14	0.375	200	0.668	60	3.247
η	15	0.5	200	0.683	60	3.225
	16	0.75	200	0.673	60	2.843
	17	1.00	200	0.684	60	2.708
	18	1.313	200	0.688	60	2.438
	19	0.75	50	0.677	15	2.087
	20	0.75	100	0.684	30	2.298
p_{av}	21	0.75	150	0.674	45	2.526
	22	0.75	200	0.672	60	3.011
	23	0.75	250	0.685	75	2.847
	24	0.75	300	0.66	90	3.103

Test conditions of each test are summarized in Table 1. As discussed in Section 3, a constant value for the strain amplitude and void ratio is considered to obtain a fully explicit model response.

Originally, values of e_0 of the test series were reported in (Wichtmann, 2005) as ranges except for test IDs 7-12, in which e_0 was the controlled test variable. However, preliminary simulations for this work showed that the model response was highly sensitive to changes in e_0. A single value was determined for each test by graphically matching the response using e_0 values within the originally reported range to those reported in (Wichtmann, 2005). This process was followed for all tests except IDs 7-12. Strain amplitudes ε_{ampl} were not available at every control cycle, as reported by (Wichtmann, 2005) and (Pasten et al., 2013). Rather, the mean observed cycle strain amplitude over all control cycles in each test was considered.

3. Soil model description

The high-cycle accumulation model (HCA) studied in this work was published by Niemunis et. al. (Niemunis et al., 2005) and presented in detail by Wichtmann (Wichtmann, 2005). In the latter, the model was originally developed in an implicit-explicit simulation scheme consisting of implicit control cycles (*N*) to verify the void ratio and strain levels and explicit calculation of accumulated strain between them. This approach allowed the model to generate accurate predictions for observed test data. The role of the control cycles was to update the values of void ratio e_N and strain amplitude $\varepsilon_{ampl}(N)$, which in turn updated the HCA model between control cycles. Additionally, HCA model parameters were initially calibrated one-at-a-time at each control cycle, resulting in a set of *N*-dependent values in an implicit-explicit scheme. At each control cycle, an implicit model needed to be executed for that reason (e.g., the hypoplastic model extended by intergranular strain developed by Niemunis (Niemunis, 2003) was considered in (Wichtmann, 2005)). An explicit-only scheme was later adopted for simulation, to avoid the computational cost due to the number of strain increments and the need to execute the full finite element (FE) model in each cycle of implicit models. In this scheme, Wichtmann (Wichtmann, 2005) considered constant mean values of void ratio $\bar{e}_N$ and strain amplitude $\bar{\varepsilon}_{ampl}$ for simulation. Then, *N*-independent HCA model parameters were calibrated in a one-at-a-time basis and proposed for simulation.

The diagram in Fig. 1 illustrates the comparison between calibration approaches adopted by (Wichtmann, 2005) and by this work. It can be noted that the first stage of simulation in both studies was to determine the initial conditions and obtain the strain at the first cycle, through the implicit model. The first approach in (Wichtmann, 2005) then updated e_N and ε_{ampl} in the implicit-explicit scheme and the model was calibrated at each *N*, thus involving *N*-variable soil conditions and HCA model parameters. In the second approach, soil conditions and HCA parameters were not updated at each *N*, instead the constant (average) values $\bar{e}_N$ and $\bar{\varepsilon}_{ampl}$ were obtained from observed data and used for explicit-only simulation. This scheme resulted in a convenient set of constant HCA model parameters, albeit at the cost of losing model accuracy according to prediction errors reported by (Wichtmann, 2005).

In this work, as shown in Fig. 1b, after determining the initial soil conditions, these were kept constant in an explicit-only scheme, to assess the viability of estimating sets of HCA model parameters simultaneously, rather than in a one-at-a-time basis. As accumulated strain predictions obtained from the former scheme were unsatisfactory, according to the discussion in Section 5.2.1, the *N*-dependent parameter estimation was carried out, achieving accurate strain predictions at each *N*. Both approaches were studied in a Bayesian framework to obtain probability density functions (PDF) for HCA model parameters instead of deterministic parameter values. Following the estimation of *N*-dependent parameter PDFs, they were combined through their conflation (Hill, 2011), which is defined in detail in Section 5.1, to obtain an *N*-independent, *N*-weighted, set of PDFs for model simulation. The strain

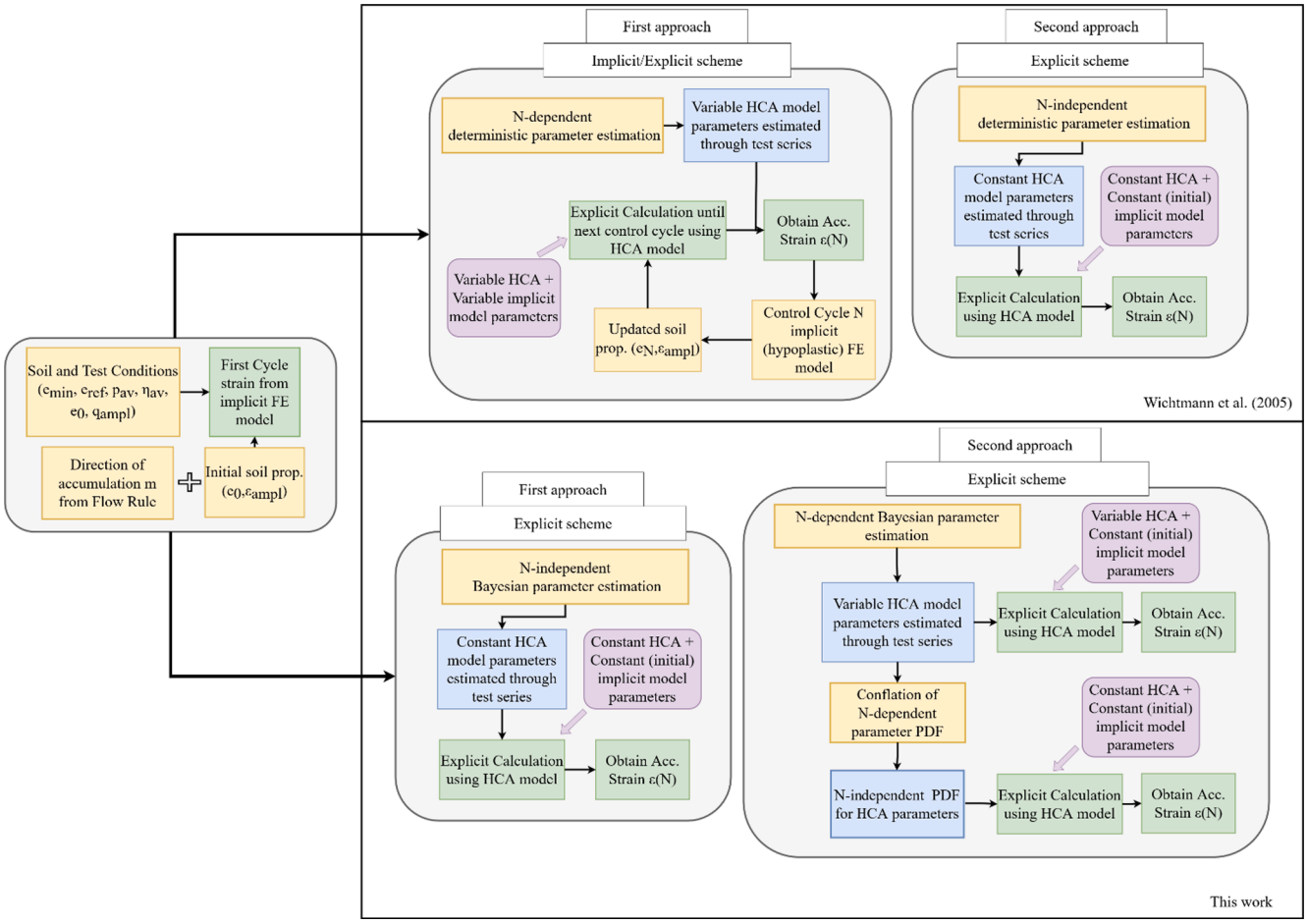

Fig. 1. Diagram comparing the high-cycle accumulation model and methodology defined by (a) Wichtmann et al. (2005) and (b) this work.

predictions were assessed in Section 5.3. The combined PDF is then validated in Section 5.4 against experimental data not used in calibration.

3.1. Model formulation

The HCA model is constructed by functions that describe different aspects of the soil behavior. In the model expression, shown in eq. (1), the accumulated strain vector $\dot{\boldsymbol{\varepsilon}}_{acc}$ is computed as the product between functions $f_{\text{ampl}}, f_e, f_p, f_Y, \dot{f}_N$, and f_π and strain direction $\mathbf{m}$ obtained from a cyclic flow rule. The function describing strain polarization f_π was considered as 1 in this study.

$$\dot{\boldsymbol{\varepsilon}}_{acc} = \dot{\varepsilon}_{acc}\mathbf{m} = f_{\text{ampl}} f_e f_p f_Y \dot{f}_N f_\pi \mathbf{m} \tag{1}$$

Strain accumulation rate $\dot{\varepsilon}_{acc}$ in eq. (1) is determined by the product of the HCA model functions, each of which is defined by a feature of the soil and the state of stress. Table 2 summarizes the formulation of each function implemented in this work, along with its respective HCA parameter for sand No. 3.

The functions in Table 2 depend on soil properties and test conditions. The first function f_{ampl} depends on the cyclic strain amplitude ε_{ampl} and its associated constant C_{ampl}, which was originally a constant value equal to 2 (Wichtmann, 2005). In a later work, Wichtmann et. al (Wichtmann et al., 2015) showed that including the parameter C_{ampl} was necessary. The reference strain amplitude ε^{ref}_{ampl} is used to normalize values of f_{ampl}. The function f_N depends on the parameters C_{N1}, C_{N2}, C_{N3}, and the number of loading cycles N. The third function, f_p depends on mean pressure p_{av} and the parameter C_p. A reference pressure p_{ref} of 100 kPa is used to normalize the value of p_{av}. Function f_Y is related to mean stress obliquity $\overline{Y}_{av}$ and depends on the parameter C_y. Lastly, the function associated with the void ratio, f_e, depends on the void ratio e, the parameter C_e and a reference void ratio e_{ref}. In an implicit-explicit simulation scheme, the value of e corresponds to the current void ratio $e(N)$, while in an explicit-only scheme it is fixed to a constant value. In upcoming sections, the initial void ratio e_0 is used as a constant value for e. The reference value e_{ref} corresponds to the loosest void ratio of the soil e_{max}, which for sand No. 3 is 0.874.

For all analyses in upcoming sections, the HCA model parameters were normalized such that they all had the same order of magnitude. Note that f_N was implemented rather than the differential version $\dot{f}_N$.

Table 2
HCA model functions implemented and reference values for sand No. 3. (Wichtmann et al., 2009).

Function	Parameters
$f_{ampl} = \begin{cases} \left(\frac{\varepsilon_{ampl}}{\varepsilon^{ref}_{ampl}}\right)^{C_{ampl}}, \varepsilon_{ampl} \le 10^{-3} \\ 100, \varepsilon_{ampl} > 10^{-3} \end{cases}$	$\varepsilon^{ref}_{ampl} = 10^{-4}$ C_{ampl}
$f_N = C_{N1}[ln(1 + C_{N2}N) + C_{N3}N]\dot{f}_N = \frac{C_{N1}C_{N2}}{1 + C_{N2}N} + C_{N1}C_{N3}$	C_{N1}, C_{N2}, C_{N3}
$f_p = exp\left(-C_p\left(\frac{p_{av}}{p_{ref}} - 1\right)\right)$	$p_{ref} = 100KPa$ C_p
$f_Y = exp(C_y\overline{Y}_{av})$	C_Y
$f_e = \frac{(C_e - e)^2}{1 + e}\frac{1 + e_{ref}}{(C_e - e_{ref})^2}$	$e_{ref} = 0.874$ C_e

4. Global sensitivity analysis

4.1. Sobol's indices

As a first step in the probabilistic characterization of the HCA model, global sensitivity analysis (GSA) was performed by computation of Sobol's indices (Sobol, 2001) for model parameters. Global methods assess the relationship between variance in parameter values and variance in model response, assessing the influence that each parameter has in model uncertainty. Sobol's first and total order indices quantify this effect regarding marginal and total variance induced by each parameter, respectively. Total index values are higher than first order, as they include all groups of parameters which contain the one in question, thus capturing uncertainty induced in the response by model parameter interactions.

Through Sobol's indices, a set of parameter PDFs is assessed to define prior PDFs for model calibration. In this context, an iterative process that considered different distribution types and parameters helped to explore the range of responses obtained by sampling from prior PDFs, as well as select which parameters to estimate in Section 5.

Sobol's indices for a set of parameters $\boldsymbol{p}$ are estimated through simulation, by using Janon's estimator (Janon et al., 2014), as the relationship between the variance of expected model response given $\boldsymbol{p}$ (i.e., $Var\left[E\left[\boldsymbol{Y}|\boldsymbol{X}_p\right]\right]$) and model variance (i.e., $Var[\boldsymbol{Y}]$), as shown in eq. (2).

$$S_p = \frac{Var\left[E\left[\boldsymbol{Y}|\boldsymbol{X}_p\right]\right]}{Var[\boldsymbol{Y}]} = \frac{Cov[\boldsymbol{Y}, \boldsymbol{Y}^p]}{Var[\boldsymbol{Y}]} \tag{2}$$

Which, by expansion of the terms results in the expression for Janon's estimator in eq. (3).

$$T_N^p = \frac{\frac{1}{Ns}\sum_{i=1}^{Ns} \boldsymbol{Y}_i \boldsymbol{Y}_i^p - \left(\frac{1}{Ns}\sum_{i=1}^{Ns}\left[\frac{\boldsymbol{Y}_i + \boldsymbol{Y}_i^p}{2}\right]\right)^2}{\frac{1}{Ns}\sum_{i=1}^{Ns}\left[\frac{\boldsymbol{Y}_i^2 + \left(\boldsymbol{Y}_i^p\right)^2}{2}\right] - \left(\frac{1}{Ns}\sum_{i=1}^{N}\left[\frac{\boldsymbol{Y}_i + \boldsymbol{Y}_i^p}{2}\right]\right)^2} \tag{3}$$

where Ns is the number of samples to be drawn, $\boldsymbol{Y}_i$ is the matrix containing all model responses, $\boldsymbol{Y}_i^p$ is the matrix containing model responses evaluated from the so-called shuffled parameter sample matrix $\boldsymbol{X}_p$ which is generated during the computation of Sobol's indices. The detailed process to obtain each of the terms in eq. (3) can be found in (Saltelli et al., 2008).

By letting $\boldsymbol{p} = i$, with i being any of the model parameters, first order indices are obtained. On the other hand, by letting $\boldsymbol{p} = \sim i$, i.e., all parameters except i, total Sobol's indices are obtained by eq. (4) as.

$$S_i^T = 1 - S_{\sim i} \tag{4}$$

By computing S_i^1 and S_i^T for each parameter, at each cycle number and for each of the test conditions available from experimental data, a history of global sensitivity of the model response to each parameter is established, which helps defining an adequate setup for model calibration in Section 5. The interpretation of Sobol's indices is that higher values indicate a higher level of influence of $\boldsymbol{p}$ on the model response, whereas lower values of the indices indicate a lower influence.

4.2. Sensitivity analysis results

To understand the relationship between each of the model parameters and its response, as well as the influence of the parameters at different cycle numbers and soil conditions, GSA was performed for each

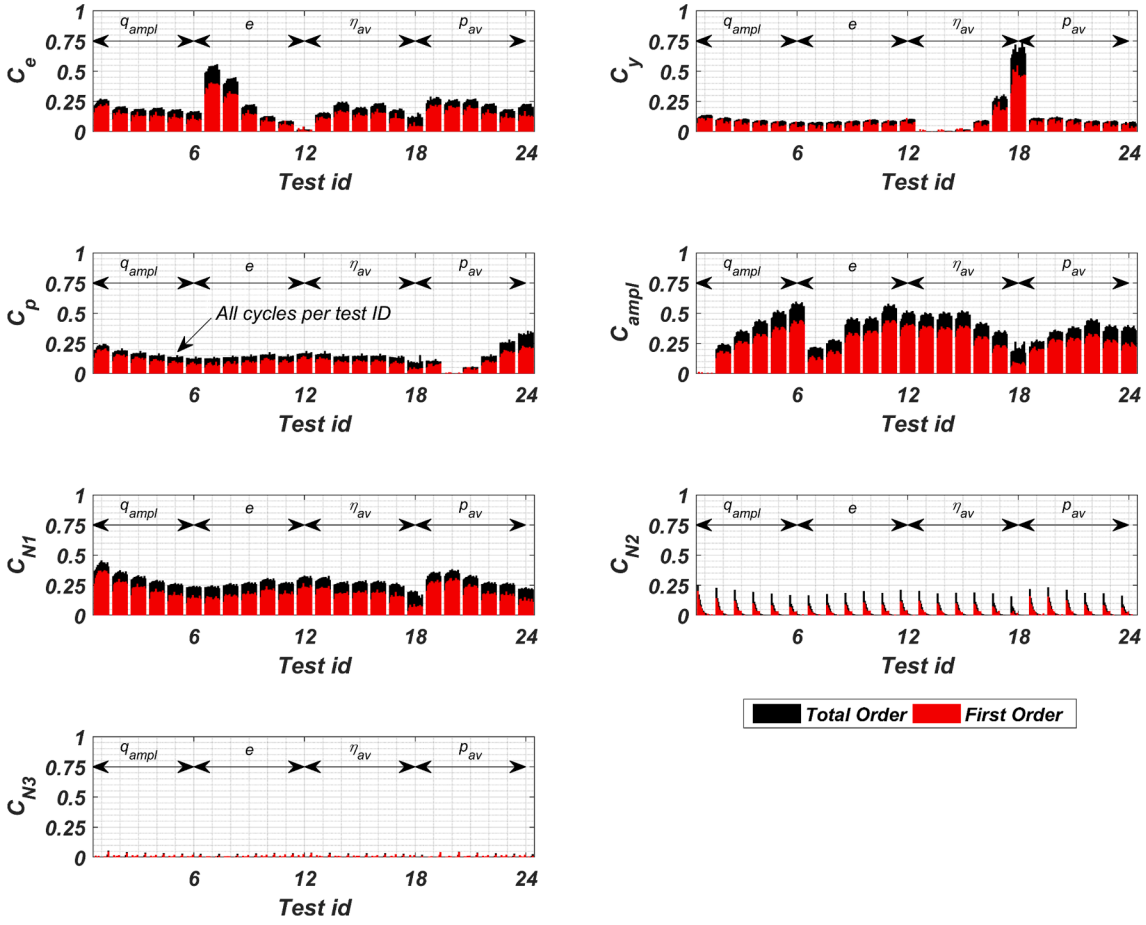

Fig. 2. Summary of Sobol's indices.

of the 24 datasets at each of the 15 cycle numbers for which experimental data was available ($N = 2, 5, 10, 20, 50, 100, 200, 500, 1000, 2000, 5000, 10000, 20000, 50000, 100000$). In the form of first and total order Sobol's indices, GSA results are summarized in Fig. 2, where each group of 15 bars correspond to the N-dependent indices of the corresponding test ID.

Parameter distributions summarized in Table 3 were used to estimate Sobol's indices through simulation, considering $Ns = 5000$ samples. A total of $Ns \times (k + 2)$ model evaluations were required for estimation of first and total order indices, with $k = 7$ parameters, adding up to 45000 evaluations for each analysis. Parameter PDFs were selected iteratively such that the range of responses obtained from sampling covered the range of observed responses in all tests.

Sobol's indices showed significant variability in parameter influence due to initial test conditions. Moreover, parameters C_e, C_y, and C_p showed a direct change of influence within the test series specifically designed to study them. C_e decreased in influence as initial void ratio e_0 increased in tests 7 to 12. Conversely, C_y gained influence as η increased in tests 13 to 18, while C_p gained influence as p_{av} increased in tests 19 to 24. The influence of C_{ampl} appeared to be proportional to the average strain amplitude in a given test, showed by the increase in the indices for tests 1 to 6 and 7 to 12 with the increase of ε_{ampl}.

The level of interaction among parameters, captured by the difference between first and total indices, appeared to be more prominent in those tests in which a given parameter had the largest influence. For example, C_y showed considerably larger difference in the indices for test 18, where it was most influential, than on test 16, where the influence of C_y was less notorious. This observation applied analogously to other parameters and could be explained by the highly non-linear model formulation. For example, in tests 6 to 12 -where e_0 was the controlling condition- the function associated with the void ratio, f_e, containing the difference between C_e and e_0 (in the explicit-only approach) could contribute a greater portion of the response compared to the other functions, thus producing a greater sensitivity to C_e when all functions were multiplied to obtain the response, as well as a greater sensitivity to the product between f_e and other functions whose values remained constant.

Secondly, parameter influence within each of the 24 tests was also investigated. While parameters related to initial test conditions did not show a considerable change in influence across cycles, those parameters related to cycle number, i.e., C_{N1}, C_{N2}, and C_{N3}, could presumably impact the response depending on the number of cycles. Regarding C_{N1}, it serves as a constant that multiples the function f_N in model formulation, although not directly multiplied by N. Consequently, its influence remained almost constant within each test, and among test conditions, showing a considerable impact on model response throughout all tests due to f_N being proportional to C_{N1}. Parameter C_{N2}, on the other hand, directly multiplied by N in model formulation, did show variability on its influence within each test, although not quite among tests. It highly impacted the model response in low cycles, while having an almost negligible effect on high-cycle responses. The influence of C_{N3} was the lowest among all parameters for the range of cycle numbers investigated, although its indices increased towards higher cycles. The purpose of this parameter in the initial formulation was to account for high number of cycles ($>10^5$), and thus its influence on the range of the available experimental data was negligible. For this reason, the data did not contain enough information about C_{N3} for it to be considered in model calibration, and it was instead fixed to a constant value $C_{N3} = 5\times10^{-5}$, according to the recommendation in (Wichtmann, 2005).

Table 3
Distributions used for GSA.

Model Parameter (Normalized units)	Distribution	Mean (μ)	Standard deviation (σ)
C_e (10^{-1})	Lognormal	4.5	1.5
C_y	Lognormal	2.5	0.5
C_p (10^{-1})	Lognormal	5.0	3.0
C_{ampl}	Lognormal	2.0	0.5
C_{N1} (10^{-4})	Lognormal	4.0	3.0
C_{N2} (10^{-1})	Lognormal	5.0	2.0
		Lower Bound	**Upper Bound**
C_{N3} (10^{-5})	Uniform	3.0	10.0

5. Bayesian parameter estimation and model calibration

5.1. Bayesian estimation setup

For model calibration, Bayesian parameter estimation is carried out in this section. Parameter posterior PDFs are obtained from Markov-Chain Monte Carlo (MCMC) simulation by sampling of parameter prior PDFs and likelihood of observed data conditioned to sampled parameters. Posteriors resulting from Bayesian estimation (BE) methods quantify the uncertainty in model response given parameter posteriors and model discrepancy definitions. With these distributions, an arbitrary number of predictions can be generated which propagate parameter uncertainty into model response. The implementation of Bayes' rule for parameter estimation is further detailed in Appendix A, and thorough reviews of Monte Carlo methods and their implementation are available in (Kroese et al., 2011) and (Wagner et al., 2022).

In this section, BE is performed for cycle-dependent and independent parameter values, the results of which are discussed in Section 5.2. Prior PDFs are assigned as the same PDFs studied through GSA in Table 3, for all parameters except C_{N3}, which is kept constant. Six model parameters are therefore estimated through MCMC, using an Adaptive Metropolis sampler (Haario et al., 2001) in a setup consisting of 4 chains of 50000 steps each, of which the last 20000 are kept for posterior PDFs. The MCMC setup is summarized in Table 4. Chains are combined after assessing their convergence through the potential reduction factor MPRSF (Gelman & Rubin, 1992), yielding a single posterior sample of 80000 points for each parameter. The multivariate effective sample size (mESS) (Vats et al., 2019) and precision estimator ($\varepsilon_{\mathrm{mESS}}$) are then computed for each estimation as termination criteria for MCMC. Finally, 1000 samples from the posterior are simulated to assess the uncertainty in model responses produced when sampling from the posterior. The model is also evaluated at the posterior mean to generate a point estimate prediction and compute its relative root mean squared error RRMSE with respect to the experimental data, as defined in eq. (5).

$$\mathrm{RRMSE}(\%) = \frac{\sqrt{\frac{1}{N_p}\sum\left(\boldsymbol{y}_{obs} - \boldsymbol{y}_{mod}\right)^2}}{\sqrt{\frac{1}{N_p}\sum \boldsymbol{y}_{obs}{}^2}} \times 100\% \tag{5}$$

where $\boldsymbol{y}_{obs}$ is the experimentally observed response, $\boldsymbol{y}_{mod}$ is the point-estimate model response, and N_p is the number of data points in each response.

For the N-dependent case, posteriors obtained are combined through conflation of distributions (Hill, 2011) to obtain a single-value PDF for model simulation. The conflation of n distributions with a set of weights w_i and probability density functions $f_i(x)$, with $i = 1, \cdots, n$ is determined by eq. (6).

$$F(x) = \frac{\prod_{i=1}^{n} f_i^{w_i/w_{max}}(x)}{\int_{-\infty}^{\infty}\prod_{i=1}^{n} f_i^{w_i/w_{max}}(t)dt} \tag{6}$$

where w_{max} is the maximum weight among PDFs. All weights w_i are

Table 4
Setup of MCMC for parameter estimation.

MCMC parameters			
Number of steps	50000 (4 chains)	**burn-in**	60%
Discrepancy σ		Constant	1% of ε_{obs}

normalized such that they sum up to 1.

5.2. Parameter estimation results

Initially, given the low effect of cycle-numbers on the influence of parameters, excluding C_{N2}, it seemed appropriate to estimate a single distribution for each parameter in each test. This stage will be referred to herein as the *N*-independent estimation, reviewed in detail in Section 5.2.1. As further discussed in that section, posteriors obtained from this approach did not generate accurate predictions overall. Moreover, they appeared to be heavily influenced by parameter priors, as opposed to by the observed data. This resulted in wide posteriors centered around the prior mean, which appeared to converge at MPRSF values lower than 1.05 but provided little to no information about the target distributions. Despite reasonable point estimates, at RRMSE levels of 8.5% in test 12 to 21% in test 19, the variance in model predictions generated by this approach was unrealistic. In a second estimation stage an *N*-dependent approach was used, which will be discussed in Section 5.2.2.

Iteratively, different prior parameters, distribution types, and definitions of the model-data discrepancy σ, represented by the standard deviation of the data likelihood, were considered for the *N*-dependent approach. For σ, cases considered constant values in strain units and constant values proportional to the observed strain. To this end, ten cases of prior and σ combinations were executed. The selected case was the one summarized in Section 5.2.2, for which the *N*-independent approach was re-evaluated to establish a comparison between both approaches. Model predictions obtained by the *N*-dependent approach were significantly more accurate than the *N*-independent approach in both point estimates and posterior samples. As opposed to the previous approach, *N*-dependent priors clearly showed convergence among chains with all MPRSF values below 1.02, and no predictions with RRMSE over 7% for a 90% confidence interval (CI). With the intention of providing a single PDF for model simulation, the *N*-dependent approach is extended in Section 5.2.2 by combining all posteriors through PDF conflation according to eq. (6).

5.2.1. Cycle-number independent analysis

For the *N*-independent case, estimation results are summarized in Table 5 while the posterior of test 16 is plotted as an example in Fig. 3. In Table 5 μ and δ refer to mean and coefficient of variation (c.o.v.), respectively. In Fig. 3, histograms of posterior MCMC samples are shown in the diagonal and colored green. A lognormal distribution fit to those samples is shown in blue and the sample mean is plotted in a black vertical line. Outside the diagonal, bivariate posterior samples from MCMC are scattered (above the diagonal) and their contours are shown (below the diagonal) along with the linear correlation coefficient between each parameter pair. Motivated by practicality, a single value for each parameter was to be estimated from each test. In other words, although the original work by Wichtmann (Wichtmann, 2005) showed that *N*-dependent parameters produced the most accurate model predictions, *N*-independent parameters are desired in practice. Naturally, this approach would produce less accurate predictions. Nevertheless, an assessment of the variability in simulated model responses was necessary to evaluate the need of considering *N*-dependent parameters.

In this stage, 24 MCMC -with 15 observed data points each- estimations were carried out with a single set of priors and MCMC setup. The priors used were the same as in Section 5.2.2 to compare the results of both approaches. For each test, model response was the complete accumulated-strain history produced by the sampled set of parameters. Given the change in sensitivity of the model response to some parameters at different strain cycles, the N-independent estimation of these parameters was expected to yield predictions that fit those cycles at which sampled parameters had the largest influence better than others. However, results showed that *N*-independent posteriors did not clearly converge to target distributions. On the contrary, most proposed samples by the Adaptive Metropolis (AM) algorithm were rejected, causing posteriors to be similar to priors despite the high variance in obtained model responses. As a side-effect, computing times for each MCMC were in the order of 5 to 6 times the cost of MCMC in the *N*-dependent approach.

Regarding parameter estimation, as shown in Table 5, posterior means of some parameters did not substantially change from prior PDF, with C_e resulting with a mean (μ) of about 4.5 and coefficient of variation, c.o.v. (δ), in the order of 33%. This pattern could also be observed for parameters C_y and C_{ampl}. Parameters C_p, C_{N1}, and C_{N2}, on the other hand, showed more variation among test IDs. Parameter C_p showed posteriors considerably narrower than its prior, with δ in the order of 17% to 30% compared to $\delta = 60\%$ in the prior. Parameter C_{N1} showed variability in posterior means across tests, with 0.42 in test 19 up to 5.0 in test 4, while posterior δ did not substantially decrease in most cases

Table 5
Summary of MCMC for the *N*-independent estimation.

	C_e (10^{-1})		C_y		C_p (10^{-1})		C_{ampl}		C_{N1} (10^{-4})		C_{N2} (10^{-1})		RRMSE	mESS	ε_{mESS}	MPRSF
Test ID	μ	δ (%)	μ	δ (%)	μ	δ (%)	μ	δ (%)	μ	δ (%)	μ	δ (%)	(%)		(%)	
1	4.49	33.0	2.52	20.1	2.44	24.5	1.99	24.5	4.69	68.6	2.18	40.2	14.51	2859	7.0%	1.029
2	4.50	33.4	2.57	20.5	2.51	25.5	2.08	25.0	4.12	59.6	1.71	30.7	10.78	1884	8.6%	1.026
3	4.44	33.1	2.54	19.8	2.54	25.7	2.06	23.5	4.50	62.3	1.14	26.6	11.92	1420	10.0%	1.041
4	4.52	34.5	2.50	19.7	2.81	27.0	2.07	24.1	5.00	83.3	1.12	26.0	17.27	1574	9.5%	1.080
5	4.43	32.9	2.55	19.4	2.88	26.1	2.03	23.1	4.10	59.7	1.28	26.2	12.24	1723	9.0%	1.033
6	4.69	33.0	2.56	19.9	2.77	26.7	2.11	24.5	4.13	54.1	1.05	21.8	13.26	1270	10.5%	1.049
7	4.58	32.3	2.48	20.2	4.59	16.9	1.96	25.3	3.50	66.1	4.03	39.6	15.00	3058	6.8%	1.013
8	4.48	31.9	2.49	20.6	3.75	20.9	1.97	25.6	3.51	65.5	2.97	38.8	13.99	2739	7.2%	1.053
9	4.50	32.2	2.53	19.7	2.91	24.7	2.07	23.5	4.04	59.7	1.98	31.7	12.83	1827	8.8%	1.082
10	4.40	31.5	2.57	19.7	2.45	27.6	2.09	23.5	4.59	54.6	1.16	23.9	10.80	1662	9.2%	1.023
11	4.52	32.1	2.65	19.3	2.33	30.0	2.16	22.4	4.94	59.5	0.57	18.6	11.92	873	12.7%	1.100
12	4.50	33.3	2.58	19.7	1.95	31.9	2.31	21.1	5.53	48.5	0.34	16.9	8.51	907	12.5%	1.083
13	4.47	32.2	2.50	19.9	2.41	28.0	2.15	24.0	4.56	61.7	1.32	30.0	12.15	1754	9.0%	1.039
14	4.43	33.2	2.52	21.0	2.85	27.3	2.07	24.5	4.26	63.2	1.58	32.6	11.96	1814	8.8%	1.101
15	4.52	35.9	2.53	20.1	2.78	26.8	2.09	22.9	4.64	62.1	1.42	31.2	13.71	1877	8.7%	1.065
16	4.46	33.5	2.51	19.5	2.78	26.3	2.07	23.9	4.21	64.3	2.27	29.8	14.59	1733	9.0%	1.037
17	4.45	32.0	2.51	19.3	2.78	26.2	2.05	22.5	4.23	58.5	1.23	23.7	14.66	1484	9.7%	1.037
18	4.49	31.2	2.55	18.0	2.83	27.3	2.08	23.9	3.96	54.4	0.43	14.2	17.25	933	12.3%	1.678
19	4.76	30.7	2.17	18.7	1.47	35.3	1.45	19.8	0.42	32.2	0.76	28.9	21.15	1005	11.8%	1.028
20	4.79	31.1	2.24	18.3	4.97	57.5	1.50	20.5	0.69	27.9	0.68	27.9	17.87	1095	11.3%	1.013
21	4.59	33.2	2.46	18.8	4.44	31.2	1.95	23.3	3.12	59.0	1.93	33.0	13.51	1905	8.6%	1.063
22	4.51	34.6	2.52	20.1	2.82	25.9	2.04	23.4	3.92	57.0	2.47	30.8	13.00	1768	8.9%	1.038
23	4.58	35.5	2.52	19.7	2.14	22.8	2.14	23.6	4.71	58.7	2.36	32.5	11.93	1754	9.0%	1.043
24	4.45	32.8	2.55	20.3	1.83	20.7	2.15	24.6	4.76	59.6	2.61	32.4	14.49	1507	9.7%	1.032

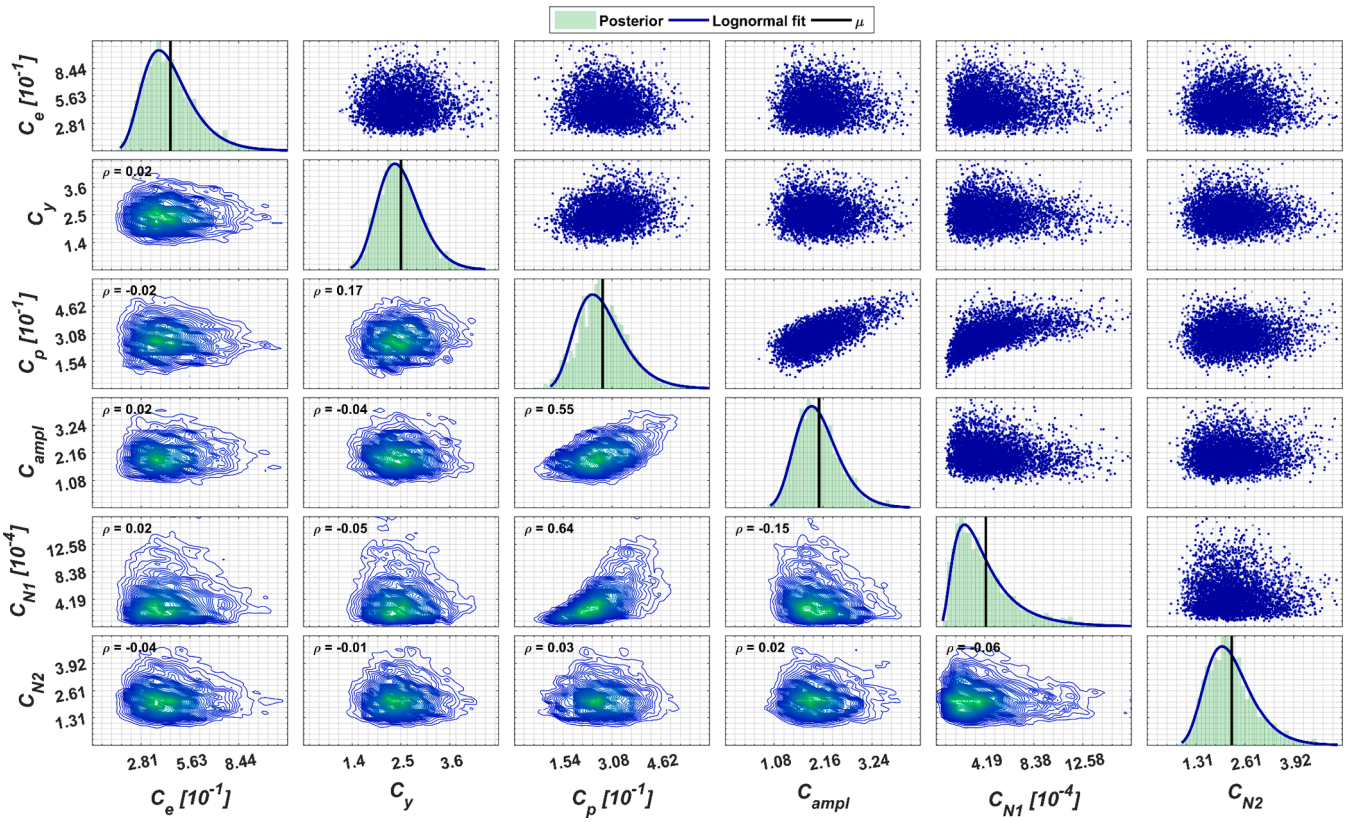

Fig. 3. Sample of parameter posteriors for the *N*-independent approach (Test ID 16 at $N = 100000$).

from the prior δ of 75%. With respect to C_{N2}, it could be observed in GSA results that its influence was most significant for low-cycle responses, with little information available for its value at high-cycles. The prior mean of 5, with a δ of 40% shifted to posterior means in the range of 0.34 in test 12, to 4.03 in test 7. Posteriors did not differ considerably from the prior, with most tests showing a δ between 30% and 40%, and the minimum being 14.2% in test 18. A significant reduction in the variability of this parameter was not expected, due to its low influence on model response. Conversely, it was not expected to induce a great degree of variance in model response at high-cycle numbers.

In general terms, point estimates corresponding to the model evaluated at the posterior mean generated predictions with RRMSE respect to experimental data in the order of 8.5 to 21%, similar to the accuracy achieved by the set of values originally proposed by Wichtmann (Wichtmann, 2005). However, the variance in simulated model responses was unrealistic in terms of strain, producing a range of responses with no application inpractice. Model predictions obtained from this approach were not included in this paper because of the large variability in the results and due to space limitations.

The *N*-independent approach, in consequence, was not satisfactory even after reaching a certain degree of convergence according to the MPRSF value obtained. Moreover, out of the 80000 MCMC steps in each posterior, effective sample sizes were in the order of 873 in test 7, for which the highest precision was obtained at 6.8% for a 95% CI, to 3058 in test 11 which showed a precision of 12.7% for the same CI. Following these results, the *N*-dependent approach was followed, as further discussed in Section 5.2.2.

5.2.2. Cycle-number dependent analysis

The *N*-dependent case considered the estimation of model parameters for each of the 15 cycle numbers for which experimental data were available. At each cycle, accumulated strains of the 24 tests were used as data for calibration. In consequence, 15 MCMC estimations with 24 data points each were carried out, as opposed to the 24 MCMC estimations with 15 data points each in the *N*-independent case. MCMC setup was the same as the previous case, with 4 chains of 50000 steps of which the last 25000 steps were combined into a single 100000-sample posterior.

Initially, a set of posteriors for each *N* was obtained, which was estimated considering all test IDs at each *N*. As opposed to the *N*-independent approach, from which 24 sets of parameters were obtained −1 for each test−, results from the *N*-dependent estimation could be considered as a single *N*-dependent set of PDFs for model parameters, which covered all tests at once. The posterior PDFs obtained were summarized in Table 6.

Parameter estimation in this case clearly showed convergence of MCMC chains, with no cases surpassing a MPRSF of 1.02. Effective sample sizes obtained were about 3 times those of the *N*-independent approach, with relative precisions ranging between 5 and 7% for a 95% CI. Point estimates obtained had variable accuracy, with decreasing RRMSE as *N* increased. For $N < 50$, in fact, errors were higher than those of the *N*-independent approach, ranging from 15 to 26% RRMSE. Moreover, for $N > 50$, point estimates achieved considerably more accurate predictions, at RRMSE of 6 to 12%. Therefore, more uncertainty in model response was expected at low *N*-values than for high *N*-values from this approach. It could be argued that less information about model parameters was contained in experimental responses during early cycles, which could be due to the small observed strains (<0.01%). In practice, extremely low strain values could be produced by several combinations of model parameters, which similarly to the *N*-independent estimation, could result in mostly rejected samples by MCMC and thus posterior PDFs similar to their priors.

With respect to parameter posteriors, it was observed that the mean value of C_e increased with respect to *N*. While for low cycles its mean was close to the prior's 4.5; the mean at high cycles was about 5.3 to 5.4. However, considerably lower δ was obtained with increasing *N*, 11.7% at $N = 2$ and 1.1% at $N = 100000$. Posteriors narrowed considerably

Table 6
Summary of MCMC for the N-dependent estimation.

	C_e (10^{-1})		C_y		C_p (10^{-1})		C_{ampl}		C_{N1} (10^{-4})		C_{N2} (10^{-1})		RRMSE	mESS	ε_{mESS}	MPRSF
N	μ	δ (%)	μ	δ (%)	μ	δ (%)	μ	δ (%)	μ	δ (%)	μ	δ (%)	(%)		(%)	
2	4.78	11.7	1.96	12.0	3.89	39.5	2.01	16.4	2.20	45.0	4.39	35.7	26.78	3835	6.1%	1.013
5	4.83	8.5	1.90	10.2	3.67	36.0	2.14	13.2	1.98	40.6	4.51	38.0	21.83	3744	6.1%	1.016
10	4.87	6.3	1.88	9.1	3.18	33.4	2.08	12.8	2.20	38.1	4.59	39.8	19.18	3351	6.5%	1.012
20	5.00	4.3	1.96	7.8	2.97	32.7	1.97	12.3	2.44	31.5	4.84	39.4	15.74	4034	5.9%	1.014
50	5.09	3.3	2.03	6.7	2.65	31.6	1.87	11.9	2.75	28.8	4.97	40.9	13.71	3735	6.1%	1.014
100	5.10	2.9	2.05	5.9	2.59	29.4	1.89	10.8	2.79	26.5	4.93	39.9	11.66	4148	5.8%	1.019
200	5.19	2.5	2.14	5.3	2.61	28.6	1.82	10.6	3.00	24.5	5.00	39.6	9.83	3539	6.3%	1.012
500	5.24	2.2	2.20	4.8	2.48	27.4	1.80	10.5	2.98	23.7	4.98	40.8	8.42	3984	5.9%	1.011
1000	5.26	2.1	2.21	4.7	2.61	26.3	1.83	9.8	2.92	22.6	4.98	40.0	8.39	4805	5.4%	1.007
2000	5.30	1.8	2.21	4.4	2.80	24.4	1.82	9.3	3.03	20.8	4.91	37.9	6.95	5201	5.2%	1.007
5000	5.34	1.7	2.16	4.3	3.26	21.1	1.84	8.7	3.24	19.3	4.97	41.3	7.17	3186	6.6%	1.014
10000	5.37	1.6	2.11	4.2	3.70	18.1	1.84	8.0	3.52	18.1	5.06	40.1	6.64	4113	5.9%	1.011
20000	5.37	1.5	2.06	4.0	4.24	15.4	1.83	8.0	3.88	17.9	5.00	40.2	6.27	5685	5.0%	1.005
50000	5.39	1.3	1.96	4.0	4.96	11.9	1.79	7.0	4.59	15.0	5.10	40.8	6.14	2814	7.1%	1.006
100000	5.40	1.1	1.85	3.8	5.24	10.0	1.71	6.4	5.21	13.1	5.06	39.1	7.33	3753	6.1%	1.010

from the prior δ of 33%, suggesting that the information in experimental data about this parameter was captured in MCMC. For other parameters, excluding C_{N2}, the same outcome was obtained. Posterior means shifted from the prior's, with δ decreasing as N increased. Parameter C_y showed little variability, ranging from 1.85 to 2.2 in posterior means, with δ decreasing from 12% to 4%, compared to the prior 20%. Parameter C_p resulted in more variable posterior means, which ranged from 2.6 to 5.2, and δ decreasing from 40% to 10% compared to prior's 60%. Parameters C_{ampl} and C_{N1} followed decreasing and increasing mean trends, respectively, with the former ranging between 2.15 and 1.7, and the latter increasing from 2.2 to 5.2 in high cycles. For both parameters, δ decreased considerably with N. While C_{ampl} showed δ ranging from 16.4% to 6.4% compared to the prior 25%, C_{N1} resulted in δ that ranged from 45% to 13.1%, compared to the 75% in its prior. Parameter C_{N2}, on the other hand, did not show clear convergence on its posteriors, even when mean values suggested an increasing trend with N. While posterior means ranged from 4.4 to 5.1, the values of δ in each N-step were similar to the prior's, at a range of 35% to 40%. Given the low influence C_{N2} had in model response for $N > 50$, it was expected that little information would be available for this parameter in experimental data. Similarly, such variability in C_{N2}, together with its influence in low strain cycles, could produce model predictions with more uncertainty at $N < 50$.

In addition to marginal posteriors for each parameter, correlations between them were also investigated during MCMC. The sample posterior shown in Fig. 4, corresponding to $N = 100000$, includes histograms for the marginal posteriors of each parameter previously discussed in the diagonal (with the MCMC sample plotted as a green histogram, a lognormal fit in blue, and posterior mean in black). Outside the diagonal, scatter plots show bivariate posteriors for parameter pairs, from which the correlation matrix was obtained for each N.

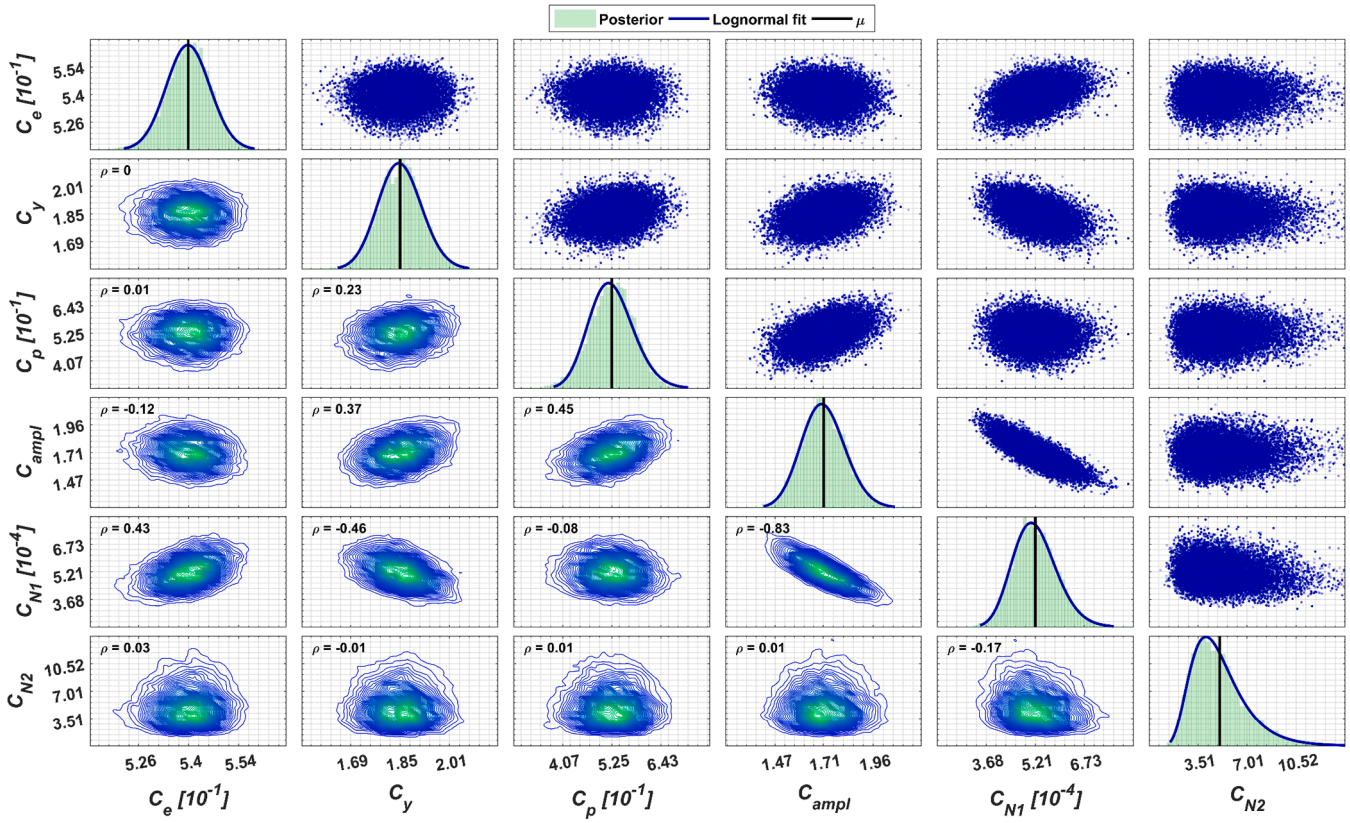

Fig. 4. Sample of parameter posteriors for the N-dependent approach (all tests at $N = 100000$).

Posteriors were sampled at each N, considering parameter correlations, to produce N-dependent predictions for each test ID which were summarized in Fig. 5. Higher accuracy was achieved by these predictions than the N-independent approach, as well as relatively low variability in model response. As expected, the uncertainty was highest in lower-strain test IDs such as tests 1 and 7, for which the RRMSE of posterior-mean samples were 18% and 27%, respectively. For most tests, posterior samples produced mean errors under 10%. In general, it was observed that N-dependent parameters allowed to reproduce observed strain in mid-strain cycles, whereas a single value for each parameter would produce a nearly bi-linear response, as was the case during the analysis in Section 5.3. Therefore, N-dependent PDFs for model parameters allowed accurate predictions in an explicit-only scheme, which could drastically reduce the computational cost of model simulation compared to the implicit/explicit simulation scheme.

Subsequent analysis focused in obtaining a more practical, single-value PDF that could adequately represent experimental data, as it was the initial purpose of the N-independent approach. For this purpose, marginal posteriors as well as their correlation matrices from the 15 estimations were combined in a manner that could reflect the amount of information that could be extracted at each N.

The lognormal fits to marginal posteriors were plotted for each parameter in Fig. 6, along with the prior distribution for reference. With the purpose of combining the information from all posteriors, cycle numbers were divided in three groups: $N = \{2, 5, 10, 20, 50, 100, 200\}$, $N = \{500, 1000, 2000, 5000\}$, and $N = \{10000, 20000, 50000, 100000\}$. These groups were colored grey, blue and green, respectively, in Fig. 6 and Fig. 7. N-dependent correlation matrices for each posterior are shown in Fig. 7. It was observed that correlations among parameters remained stable despite the changes in marginal distributions. Therefore, a single correlation matrix, shown in Table 7, was defined for sampling of the single-value PDF, as the average of all 15 cycles. Previously, samples shown in Fig. 5 had been drawn from the full N-dependent posterior, including the respective correlation matrices. Discussion in Section 5.3 includes the impact of using an average correlation matrix for sampling of the single combined distribution.

To obtain a single set of means and c.o.v. for each parameter, posterior lognormal fits were combined by conflation of distributions. This method establishes a single PDF which is more influenced by narrow posteriors and weighted by a certain of values defined by hand. In the context of this work, as high-cycle posteriors were found to be narrower than low-cycle ones, high-cycle posteriors had more influence in conflated PDF than low-cycle posteriors. Additionally, weights w_i for each posterior were defined such that for N up to 500 $w_1 = 0.4$, for N between 500 and 5000 $w_2 = 0.6$, and for N between 10000 and 100000 $w_3 = 1$. The weights were normalized such that they sum up to the unity. Different weights represent the credibility of each experiment, which was the original meaning discussed in (Hill, 2011). Herein, w_i were selected to reflect a possible level of engineering interest in each group of cycles for the conflation. Iteratively changing w_i produced the conflated PDF to lean towards one group or another. The resulting lognormal PDF was based on high-cycle posteriors more heavily than on low-cycle ones, while still including the information obtained from all MCMC.

A single-valued PDF was obtained for sampling and summarized in Table 7 along the correlation matrix obtained from the N-dependent estimation. Distribution means were similar to those proposed originally by Wichtmann (Wichtmann, 2005), while a measure of parameter uncertainty and correlations are also provided by this study.

5.3. Predicted responses

The HCA model was evaluated for each of the 24 tests through the single PDF summarized in Table 7, by drawing 1000 samples, from each parameter independently and from the correlated PDF as well. In general, the predictions obtained from the N-dependent approach showed higher accuracy than those for the N-independent approach, although the PDF generated by a higher weighting of high cycle numbers meant

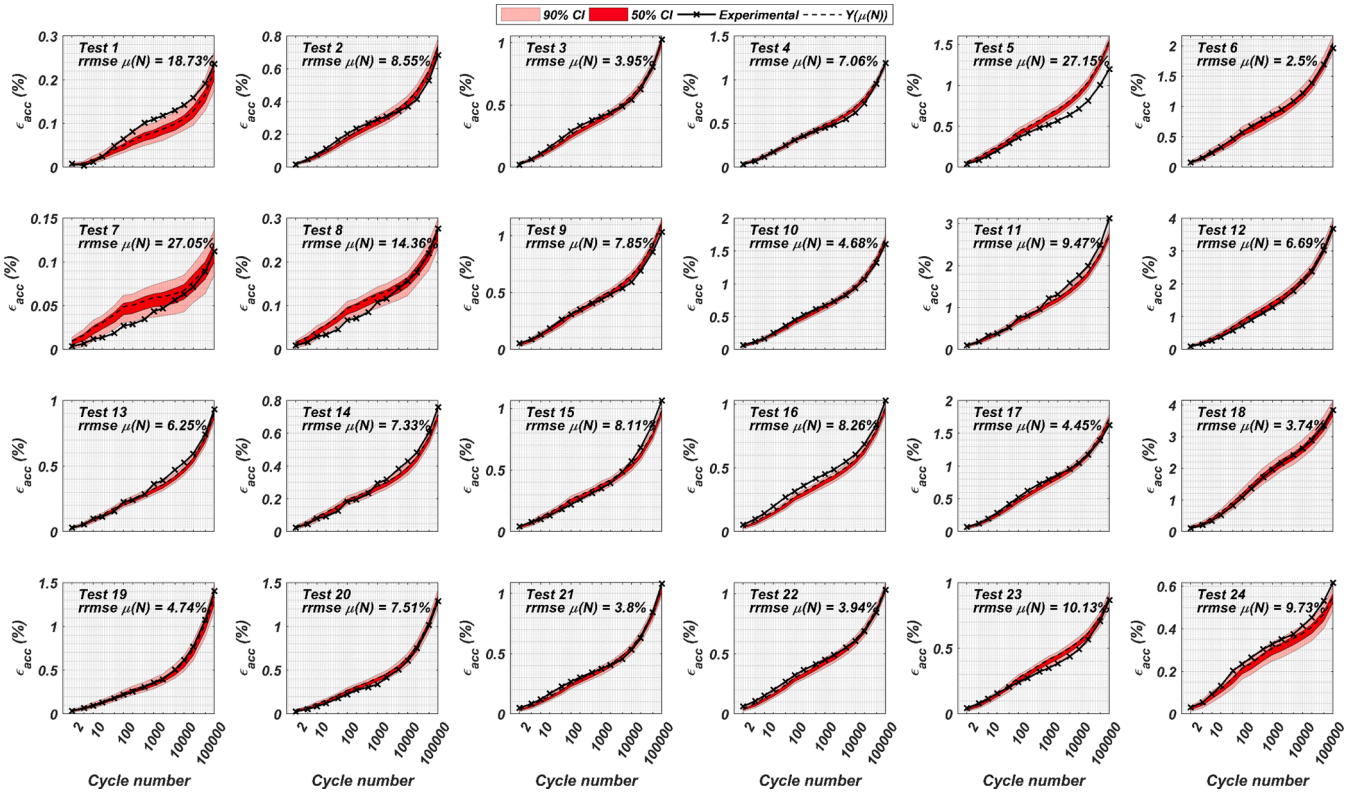

Fig. 5. Predictions obtained by drawing samples from the posterior obtained from the N-dependent approach.

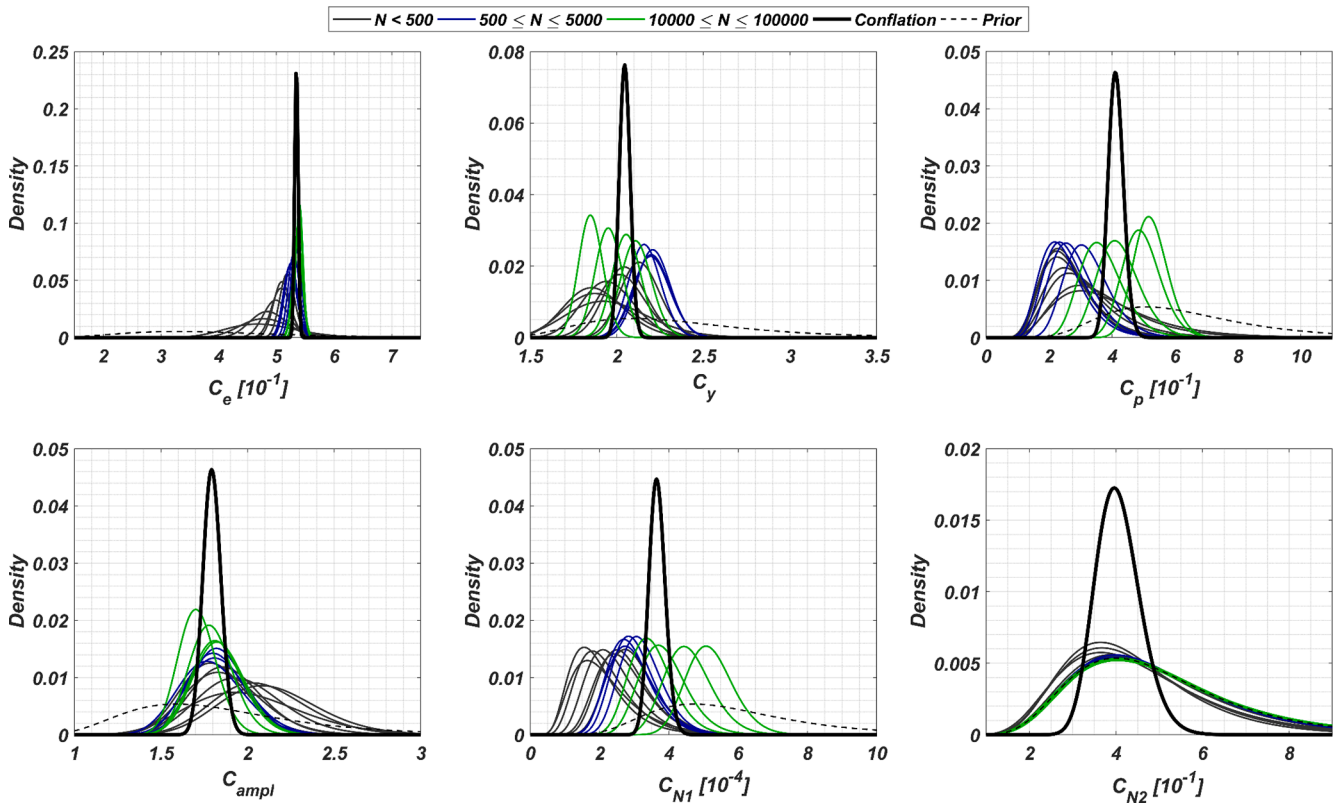

Fig. 6. Summary of parameter posteriors for the *N*-dependent case.

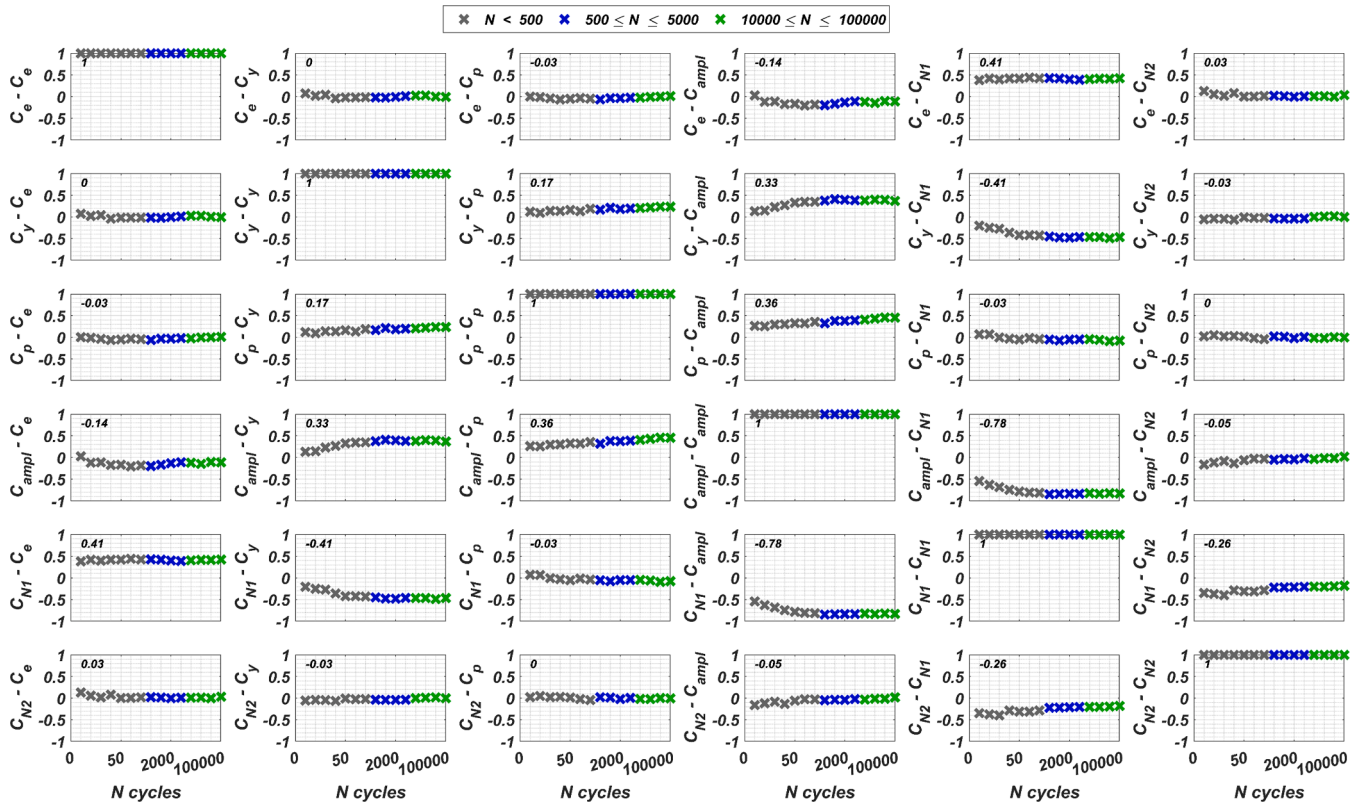

Fig. 7. Correlation matrices from each *N*-dependent estimation.

Table 7
Parameter distributions obtained from posterior conflation.

	C_e [10^{-1}]	C_y	C_p [10^{-1}]	C_{ampl}	C_{N1} [10^{-4}]	C_{N2} [10^{-1}]
Mean (μ)	5.3	2.0	4.1	1.8	3.7	4.1
Std. dev. (σ)	0.030	0.031	0.242	0.052	0.234	0.520
c.o.v. (δ)	0.6%	1.5%	5.9%	2.9%	6.4%	12.8%
	Parameter correlation matrix					
	C_e	C_y	C_p	C_{ampl}	C_{N1}	C_{N2}
C_e	1.0	0.00	−0.03	−0.14	0.41	0.03
C_y	0.00	1.0	0.17	0.33	−0.41	−0.03
C_p	−0.03	0.17	1.0	0.36	−0.03	0.00
C_{ampl}	−0.14	0.33	0.36	1.0	−0.78	−0.05
C_{N1}	0.41	−0.41	−0.03	−0.78	1.0	−0.26
C_{N2}	0.03	−0.03	0.00	−0.05	−0.26	1.0

that for tests with low accumulated strain, such as tests 1 and 24, predictions were not as accurate. In addition, the variability in model response was considerably less than that of the *N*-dependent approach. On the other hand, predictions from the conflated PDF achieved less accurate predictions than the *N*-dependent approach. There was, in consequence, a trade-off between practicality and model accuracy. However, the single PDF in both sampling cases generated predictions with low variability that approximated observed responses with point estimate errors in the range of 3.5% to 15% for 21 of the tests, and three tests with mean errors of 21 to 25%. Samples generated from uncorrelated and correlated sampling of parameters in Table 7 are shown in Fig. 8 and Fig. 9. Clearly, point estimate errors were the same in both cases as posterior means were the same. However, although the variance in uncorrelated sampling was considerably higher than that of correlated sampling, it allowed to capture a level of uncertainty that might be of interest in later probabilistic studies including this PDF. On the contrary, predictions obtained by correlated sampling of the model had little variability which meant that for those points for which predictions were not accurate at a point-estimate level, parameter distributions could not capture the observed response. Such was the case in test 16, for example, where the whole response was underestimated by the correlated PDF, whereas uncorrelated sampling came closer to covering the whole response in the 50% and 90% CI.

Additional *N*-dependent calibration scenarios were carried out, considering subsets of six and twelve tests each, and replicating the setup described in Section 5.1. These scenarios were designed to evaluate the effects of the number and type of datasets (i.e., number of tests and type of series) on the parameter estimation results and model prediction capabilities. The cases considered were selected based on subsets of one and two complete test series, as well as subsets taken randomly from the complete sample (i.e., including tests from all series). Regardless of including six or twelve test IDs, the inferred posteriors from subsets that included at least one test per series generated more accurate predictions on the whole sample than those calibrated against only one or two test series. Moreover, the information contained in the experimental data about sensitive parameters was the most decisive factor in the general predictive capacity of the calibrated model. This suggests that efforts in collecting experimental data should focus on gaining as much information as possible about sensitive model parameters.

5.4. Model validation

The conflated PDF obtained in Section 5.2.2 is used herein for sampling of the HCA model for sands. Model predictions were generated for all tests used in calibration by uncorrelated (see Fig. 10a) and correlated (see Fig. 10b) sampling of parameters, and results from both approaches were evaluated in Section 5.3. This section discusses predictions obtained by 1000 samples of the proposed single PDF, also from independent and correlated sampling, for five sets of data from tests not considered for model calibration. Experimental data from these tests is

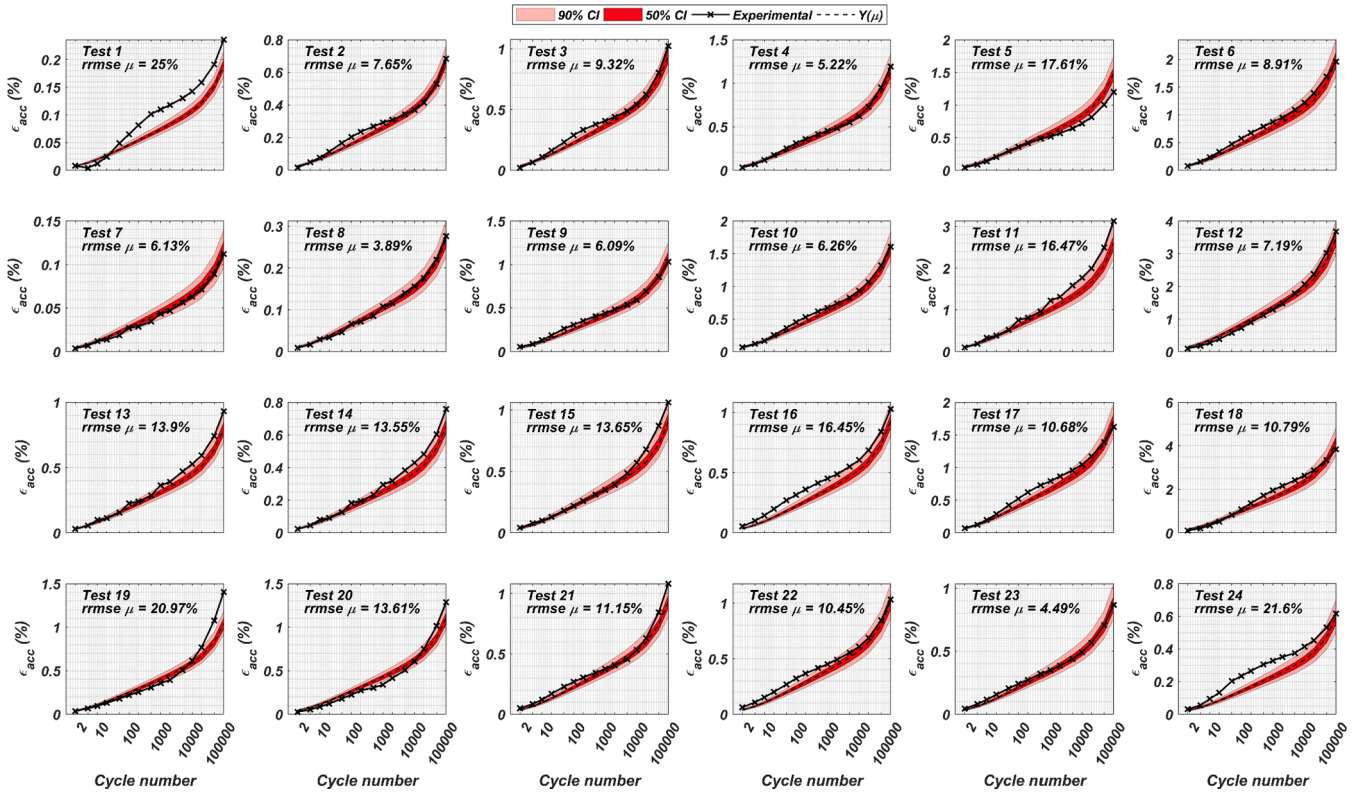

Fig. 8. Model predictions obtained from uncorrelated sampling of the conflated PDF from *N*-dependent estimation.

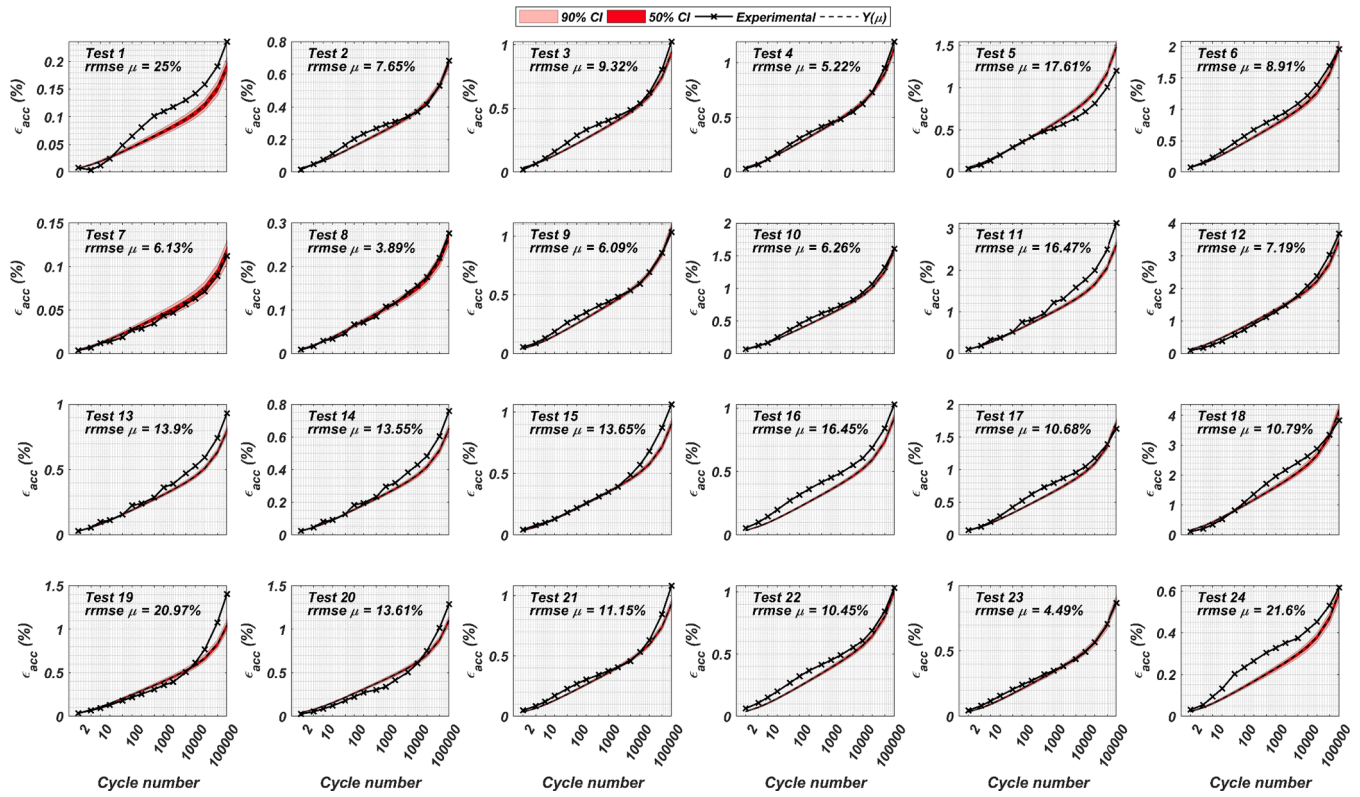

Fig. 9. Model predictions obtained from correlated sampling of the conflated PDF from *N*-dependent estimation.

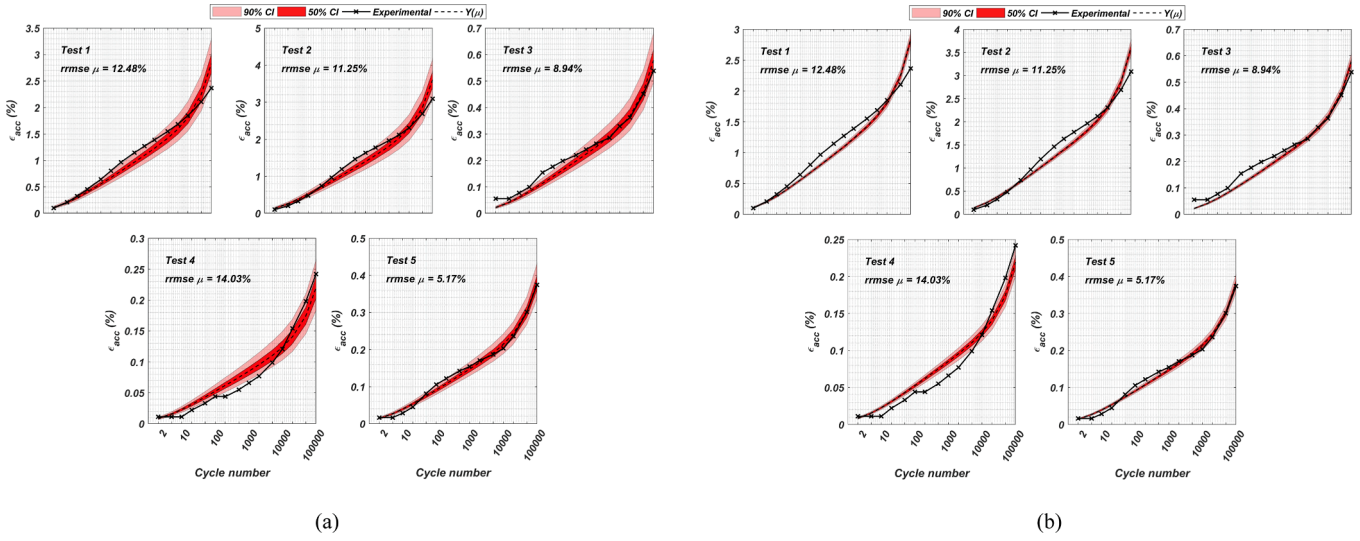

Fig. 10. Model predictions for validation datasets. (a) Uncorrelated sampling. (b) Correlated sampling.

Table 8
Experimental data considered for model validation.

Test ID	η	p_{av} (KPa)	e_0	q_{ampl} (KPa)	ε_{ampl} (10^{-4})
1	1.125	200	0.7	60	2.629
2	1.25	200	0.69	60	2.539
3	0.75	200	0.64	60	2.929
4	0.75	200	0.605	60	2.647
5	0.75	200	0.698	31	1.451
6	0.75	200	0.698	12	0.504

summarized in Table 8.

Responses generated in this stage were completely predictive as the proposed PDF was not informed by the data in these six tests. Point estimate errors were the same in both cases, analogously to responses in Section 5.3. The six tests resulted in RRMSE for point estimates between 5.2% and 14%. Therefore, the proposed PDF produced reasonably accurate mean-predictions for data at strain levels between 0.25% and 4.5%, effectively covering the range of strains for which the model was originally calibrated.

Correlation between parameters decreased response uncertainty considerably, although in some cases this meant that all predictions had a higher approximation error. The level of accuracy achieved by

uncorrelated sampling suggests that it might capture the model behavior well enough to be used in simulation. On one hand, the error of the single prediction generated by the mean of the parameter PDF does not depend on correlations. On the other hand, the expected value of model response was similar in uncorrelated and correlated sampling. Because of this, it might be more practical to sample from the proposed PDF without considering parameter correlations. Moreover, correlation matrices obtained from each single posterior in Section 5.2.2 might unreasonably reduce the model uncertainty observed in calibration, as the conflation of posteriors produced already narrow PDFs which did not necessarily include the tails of any individual posterior PDFs. In this sense, uncorrelated sampling of the single PDF is advised to reflect the parameter variance observed in calibration. At the same time, if test conditions e_0, p_{av}, η, q_{ampl} and ε_{ampl} can be confidently determined, correlated *N*-dependent sampling of the parameters will produce the best results and is therefore advised.

6. Conclusions

This paper developed a probabilistic characterization of the high cycle accumulation (HCA) model proposed by Niemunis et al. (Niemunis et al., 2005). Experimental data from the work by Wichtmann (Wichtmann, 2005) was used to calibrate model parameters through Markov-Chain Monte Carlo (MCMC) and evaluate different sampling strategies for model simulation. All computations made in this work considered an explicit-only approach to the model, because of which an implicit model was only considered for the first strain cycle. The goal of this approach was to avoid the cost of an implicit-explicit approach.

In a first stage, global sensitivity analysis (GSA) in the form of Sobol's indices was conducted to define prior distributions for calibration. Analyses were performed over the 15 cycle data points available and for each of the 24 test IDs, which revealed *N*-dependence in the influence of one parameter and varying influence of HCA parameters depending on test conditions.

Bayesian parameter estimation was then carried out with MCMC for *N*-independent and *N*-dependent cases and the posterior distributions obtained from each case were compared. Upon discarding the results obtained from *N*-independent estimations, subsequent work aimed to achieve a set *N*-independent parameters that retained prediction accuracy and a level of uncertainty that reflected that of MCMC estimations.

To this end, parameter posteriors from each cycle number were combined through the conflation of their lognormal fits and a correlation matrix was defined for sampling. The predictions generated by uncorrelated and correlated sampling of this PDF were compared in terms of point-estimate predictions with PDF means, the uncertainty in model response, and accuracy of expected value of model response.

In the presence of confidently determined test conditions, correlated sampling of *N*-dependent posteriors is advised, as they could closely replicate experimental data in most cases and were informed by all tests in each cycle number. For general use, uncorrelated sampling of the conflated PDF is advised, as point-estimate predictions achieved more accuracy than the values proposed by the original authors of the model, and it captures the uncertainty observed in MCMC.

This work presented a probabilistic calibration framework for the HCA model which employed the same series of tests proposed by the model authors, although all parameters were estimated simultaneously, as opposed to sequentially. Accumulated strain histories from each test were considered without any type of normalization, which prevented the alteration of observed data. Moreover, the process for obtaining a single-value PDF can be extended to other datasets. This eliminates the need of *N*-dependent deterministic estimation and a later criteria-based unification of parameter values. Furthermore, *N*-independent parameters in this work achieved similar-to-better results compared to the set of parameters proposed by the model authors, while providing a measure of the uncertainty in model response.

Ultimately, we consider that the explicit-only approach presented in this work for probabilistic calibration of the HCA model was successful as it captured experimental data from a wide range of test conditions in a framework that is of low computational cost and mostly automated, making it suitable for academic and engineering practice.

CRediT authorship contribution statement

M. Birrell: Conceptualization, Methodology, Software, Formal analysis, Investigation, Writing – original draft. **C. Pastén:** Conceptualization, Investigation, Writing – original draft, Writing – review & editing, Supervision. **J. Abell:** Writing – original draft, Writing – review & editing. **R. Astroza:** Conceptualization, Methodology, Investigation, Writing – original draft, Writing – review & editing, Supervision, Project administration, Funding acquisition.

Declaration of Competing Interest

The authors declare that they have no known competing financial interests or personal relationships that could have appeared to influence the work reported in this paper.

Acknowledgements

R. Astroza and C. Pastén acknowledge the support from the Chilean National Research and Development Agency (ANID), FONDECYT projects No. 1200277 and 1190995, respectively. M. Birrell acknowledges the support of ANID through Beca Doctorado Nacional No. 21210182.

Appendix A. Bayesian parameter estimation

Bayesian inversion as implemented in this work, looks to infer a vector of model parameters $\boldsymbol{\theta}$ defining a certain model class $\boldsymbol{M}$, from a set of observed data $\mathbf{y_{obs}} = \{y_{j,k} / j = 1,..,N_{obs}, k = 1,..,N_{out}\}$, where N_{obs} is the number of observations and N_{out} is the number of points in each observation. From Bayes' theorem, the posterior distribution for $\boldsymbol{\theta}$ is defined by.

$$P(\theta|\mathbf{y_{obs}}) = \frac{P(\mathbf{y_{obs}}|\theta)P(\theta)}{P(\mathbf{y_{obs}})} \tag{A.1}$$

Where $P(\theta|\mathbf{y_{obs}})$ is the posterior distribution of $\boldsymbol{\theta}$, $P(\theta)$ is the prior distribution of $\boldsymbol{\theta}$, $P(Y_{obs}|\theta)$ is the likelihood of $\boldsymbol{M}$ predicting $\mathbf{Y_{obs}}$ through $\boldsymbol{\theta}$, and $P(\mathbf{y_{obs}}) = P(\mathbf{y_{obs}}|\boldsymbol{M}) = \int_{-\infty}^{\infty} P(\mathbf{y_{obs}}|\theta)P(\theta)d\theta$ is the model evidence and normalizes the posterior such that it integrates to 1.

These distributions combine the prior beliefs about the value of $\boldsymbol{\theta}$ with the information inferred from the data through the likelihood function, which, if independence between observations is assumed, can be written as $P(\mathbf{y_{obs}}|\theta) = \prod_{k=1}^{N_{obs}} P\left(\mathbf{y_{obs},k}|\theta\right)$. In consequence, the posterior combines the likelihood inferred from experimental data with the prior beliefs about parameter values, effectively making the posterior an "updated" belief. It might be useful to consider different cases of prior distributions for this reason, including which provide more or less information about $\boldsymbol{\theta}$.

From the likelihood function, it can be noted that the number of observations may have an impact on the posterior, associated with the variability between observations. For example, given that a larger number of observations implies a decrease in the marginal contribution of each observation to

the posterior, larger variability in the observations may result in a wider posterior. Therefore, an adequate dataset should be selected for updating, in order to make the most out of this framework.

Usually, the likelihood of data is assumed to follow a normal distribution with a variance term σ^2 referred to as model discrepancy. It represents the non-modeled sources of model error in $\boldsymbol{M}$ and the measurement noise. This term might be modeled as a random variable or considered constant. Again, it might be useful to assess the sensitivity of the posterior to model discrepancy. For example, a larger value of σ may be less restrictive towards posterior convergence, but at the same time return more uncertain predictions.

In practice, an analytical approach is not feasible to solve the expression (A.1) for computer models, so a simulation approach is taken. To this end, Markov-Chain Monte Carlo (MCMC) is used in this work. Multiple chains are sampled from the posterior by proposing updates to the prior distribution. At each step, the posterior distribution is evaluated on the proposed sample, with rejection criteria based on the model fit to the observed data. Multiple sampling algorithms are available for MCMC, in this work the Adaptive Metropolis algorithm (Haario et al., 2001) is used. Depending on the stochastic model (i.e., selection of priors, likelihood parameters, set of observations) the chains may or not satisfactorily converge to a stationary distribution in a number of steps. To assess the convergence of chains, the multivariate potential scale reduction (MPSRF) (Gelman & Rubin, 1992) is considered in this work. To assess the quality of the inference, the multi-chain effective sample size is considered and compared to the minimum effective sample size for a given confidence interval and Monte Carlo error (Vats et al., 2019). Bayesian estimation methods are employed in a wide range of geotechnical engineering applications, for example in (Astroza et al., 2017), (Rahimi et al., 2019), (Zheng et al., 2018), (Jin et al., 2021).

References

Aladejare, A.E., Wang, Y.u., 2018. Influence of rock property correlation on reliability analysis of rock slope stability: From property characterization to reliability analysis. Geosci. Front. 9 (6), 1639–1648.

Astroza, R., Pastén, C., Ochoa, F., 2017. Site response analysis using one-dimensional equivalent-linear method and Bayesian filtering. Comput. Geotech. 89, 43–54.

Birrell, M., Astroza, R., Carreño, R., Restrepo, J.I., Araya-Letelier, G., 2021. Bayesian parameter and joint probability distribution estimation for a hysteretic constitutive model of reinforcing steel. Struct. Saf. 90, 102062.

Chong, S.-H., Pasten, C., 2018. Numerical study on long-term monopile foundation response. Mar. Georesources Geotechnol. 36 (2), 190–196.

Christian, J., 2004. How Well Do We Know What We Are Doing? J. Geotech. Geoenviron. Eng. 130, 985–1003.

Corti, R., Diambra, A., Wood, D.M., Escribano, D.E., Nash, D.F.T., 2016. Memory Surface Hardening Model for Granular Soils under Repeated Loading Conditions. J. Eng. Mech. 142 (12), 04016102.

Cuéllar, P., Mira, P., Pastor, M., Fernández Merodo, J.A., Baeßler, M., Rücker, W., 2014. A numerical model for the transient analysis of offshore foundations under cyclic loading. Comput. Geotech. 59, 75–86.

Francoise, S., Karg, C., Haegeman, W., Degrande, G., 2006. A numerical model for foundation settlements due to deformation accumulation in granular soils under repeated small amplitude. Int. J. Numer. Anal. Meth. Geomech. 30, 1303–1336.

Gelman, A., Rubin, D., 1992. Inference from iterative simulation using multiple sequences. Statistical science 7 (4), 457–511.

Haario, H., Saksman, E., Tamminen, J., 2001. An adaptive Metropolis algorithm. Bernoulli 7, 223–242.

Hill, T.P., 2011. Conflations of probability distributions. Trans. Am. Math. Soc. 363 (6), 3351–3372.

Houlsby, G.T., 2016. Interactions in offshore foundation design. Interactions in offshore foundation design. Géotechnique 66 (10), 791–825.

Janon, A., Klein, T., Lagnoux, A., Nodet, M., Prieur, C., 2014. Asymptotic normality and efficiency of two Sobol index estimators. ESAIM: Probab. Statist. 18, 342–364.

Jin, Y., Biscontin, G., Gardoni, P., 2021. Adaptive prediction of wall movement during excavation using Bayesian inference. Comput. Geotech. 137, 104249.

Jin, Y.-F., Yin, Z.-Y., Zhou, W.-H., Horpibulsuk, S., 2019. Identifying parameters of advanced soil models using an enhanced transitional Markov chain Monte Carlo method. Acta Geotech. 14 (6), 1925–1947.

Jin, Y.-F., Yin, Z.-Y., Zhou, W.-H., Liu, X., 2020. Intelligent model selection with updating parameters during staged excavation using optimization method. Acta Geotech. 15 (9), 2473–2491.

Jostad, H.P., Dahl, B.M., Page, A., Sivasithamparam, N., Sturm, H., 2020. Evaluation of soil models for improved design of offshore wind turbine foundations in dense sand. Géotechnique 70 (8), 682–699.

Kroese, D., Taimre, T., Botev, Z.I., 2011. Handbook of Monte Carlo Methods. John Wiley and Sons, New York.

Liu, H.Y., Abell, J.A., Diambra, A., Pisanò, F., 2019. Modelling the cyclic ratcheting of sands through memory-enhanced bounding surface plasticity. Geotechnique 69 (9), 783–800.

Liu, H., Kementzetzidis, E., Abell, J.A., Pisanò, F., 2021. From cyclic sand ratcheting to tilt accumulation in offshore monopiles: 3D FE modelling using SANISAND-MS. Géotechnique.

Machaček, J., Wichtmann, T., Zachert, H., Triantafyllidis, T., 2018. Long-term settlements of a ship lock: Measurements vs. FE-prediction using a high cycle accumulation model. Comput. Geotech. 97, 222–232.

Mercado, V., Ochoa-Cornejo, F., Astroza, R., El-Sekelly, W., Abdoun, T., Pastén, C., Hernández, F., 2019. Uncertainty quantification and propagation in the modeling of liquefiable sands. Soil Dyn. Earthq. Eng. 123, 217–229.

Miro, S., König, M., Hartmann, D., Schanz, T., 2015. A probabilistic analysis of subsoil parameters uncertainty impacts on tunnel-induced ground movements with a back-analysis study. Comput. Geotech. 68, 38–53.

Niemunis, A., 2003. Extended hypoplastic models for soils. Des institutes für grundbau und bodenmechanik der ruhr-universität Bochum, Bochum.

Niemunis, A., Wichtmann, T., Triantafyllidis, T.h., 2005. A high-cycle accumulation model for sand. Comput. Geotech. 32 (4), 245–263.

Otake, Y., Shigeno, K., Higo, Y., Muramatsu, S., 2021. Practice of dynamic reliability analysis with spatiotemporal features in geotechnical engineering. Georisk 1–16.

Pasten, C., Shin, H., Santamarina, J.C., 2013. Long-Term Foundation Response to Repetitive Loading. J. Geotech. Geoenviron. Eng. 140 (4), 04013036.

Rahimi, M., Shafieezadeh, A., Wood, D., Kubatko, E.J., Dormady, N.C., 2019. Bayesian calibration of multi-response systems via multivariate Kriging: Methodology and geological and geotechnical case studies. Eng. Geol. 260, 105248.

Saltelli, A., Ratto, M., Andres, T., Campolongo, F., Cariboni, J., Gatelli, D., Saisana, M., Tarantola, S. (Eds.), 2008. Global Sensitivity Analysis. The Primer. John Wiley & Sons, Ltd, Chichester, UK.

Sobol, I.M., 2001. Global sensitivity indices for nonlinear mathematical models and their Monte Carlo estimates. Math. Comput. Simul. 55 (1–3), 271–280.

Staubach, P., Machaček, J., Tschirschky, L., Wichtmann, T., 2021. Enhancement of a high-cycle accumulation model by an adaptive strain amplitude and its application to monopile foundations. Int. J. Numer. Anal. Meth. Geomech. 46 (2), 315–338.

Suchomel, R., Mašín, D., 2011. Probabilistic analyses of a strip footing on horizontally stratified sandy deposit using advanced constitutive model. Comput. Geotech. 38 (3), 363–374.

Suiker, A., Borst, R.D., 2003. A numerical model for the cyclic deterioration of railway tracks. Int. J. Numer. Methods Eng. 57, 441–470.

Vats, D., Flegal, J.M., Jones, G.L., 2019. Multivariate output analysis for markov chain monte carlo. Biometrika 106 (2), 321–337.

Wagner, P.R., Nagel, J., Marelli, S., Sudret, B., 2022. UQLab user manual - Bayesian inference for model calibration and inverse problems. Chair of Risk, Safety and Uncertainty Quantification, ETH, Zurich.

Whitman, R.V., 1984. Evaluating calculated risk in geotechnical engineering. J. Geotech. Eng. 110 (2), 143–188.

Wichtmann, T., 2005. Explicit accumulation model for non-cohesive soils under cyclic loading, s.l.: PhD Thesis.

Wichtmann, T., Niemunis, A., Tiantafyllidis, T., 2015. Improved simplified calibration procedure for a high-cycle accumulation model. Soil Dyn. Earthquake Eng. 70, 118–132.

Wichtmann, T., Niemunis, A., Triantafyllidis, T., 2009. Validation and calibration of a high-cycle accumulation model based on cyclic triaxial tests on eight sands. Soils Found. 49 (5), 711–728.

Wichtmann, T., Niemunis, A., Triantafyllidis, T., 2010. On the determination of a set of material constants for a high-cycle accumulation model for non-cohesive soils. Int. J. Numer. Anal. Meth. Geomech. 34 (4), 409–440.

Zheng, D., Huang, J., Li, D.-Q., Kelly, R., Sloan, S.W., 2018. Embankment prediction using testing data and monitored behaviour: A Bayesian updating approach. Comput. Geotech. 93, 150–162.

Zhou, W.-H., Yin, Z.-Y., Yuen, K.-V. (Eds.), 2021. Practice of Bayesian Probability Theory in Geotechnical Engineering. Springer Singapore, Singapore.

Zhou, W., Tan, F., Yuen, K., 2018. Model updating and uncertainty analysis for creep behavior of soft soil. Comput. Geotech. 100, 135–143.